Light-driven motion of charged domain walls in isolated ferroelectrics

Jonathan Ordoñez-Pimentel,[1,2] Michel Venet,[2] Diego A. Ochoa,[1]
Fernando Rubio-Marcos,[3,4] José F. Fernández,[3] and José E. García[1]

[1] *Department of Physics, Universitat Politècnica de Catalunya, 08034 Barcelona, Spain*
[2] *Department of Physics, Universidade Federal de Sao Carlos, 13565-905 Sao Carlos, Brazil*
[3] *Department of Electroceramics, Instituto de Cerámica y Vidrio - CSIC, 28040 Madrid, Spain*
[4] *Escuela Politécnica Superior, Universidad Antonio de Nebrija, 28040 Madrid, Spain*

(Dated: December 12, 2022)

Light-induced ferroelectric domain wall motion turns out to be a promising phenomenon to develop new photo-controlled devices. However, the physical origin of this ligh-matter coupling when material is irradiated with visible light remains unclear. Here, a phenomenological model predicting the motion of charged domain walls (CDWs) is developed. The photo-induced electronic reconstruction mechanism is proposed as the primary absorption mechanism, leading to a linear dependence for the polarization perturbation with the light intensity. Domain walls motion is then driven by the energetic difference between domains in a CDW array, such that the macroscopic polarization can be easily tuned.

I. INTRODUCTION

Domain walls are known to be functional interfaces to control the macroscopic polarization of ferrolectrics [1, 2]. These interfaces move through external stimuli, typically electric field or mechanical stress, thereby yielding domains reconfiguration. Recently, however, polarization control via optical excitation has become a highly appealing topic because it entails new paradigms for technology [3–8]. Optical switching mechanisms include (piezo)photovoltaic effect [9–11] as well as a variety of experimentally observed phenomena based on the light control of ferroelectrics domains [12–14].

In this context, the light driven motion of ferroelectric domain walls provides versatile phenomenology that could potentially power the next generation of photoferroelectric devices. However, the major drawback for achieving an effective reversible optical control of domains rearrangement in conventional ferroelectrics lies in their wide optical band gap, typically greater than 3 eV; therefore, irradiating with UV-light turns out to be mandatory [8, 15]. Nevertheless, recent studies have evidenced the ability to move ferroelectric domain walls when a low-power ($<$ 100mW) visible light impinges on an isolated barium titanate (BTO) single crystal [16]. Due to the domains reconfiguration, macroscopic properties such as dielectric permittivity or mechanical strain can be photo-controlled showing a linear dependence with the light intensity at several wavelengths in the visible spectrum [17, 18].

Although convincing experimental findings have pointed out that the photo-induced ferroelectric domain rearrangement is primary linked to strong charged domain walls (CDWs) [17, 19], the physical origin of this manifestation of light-matter coupling remains unclear so far. It was postulated, but not formally developed, the charge accumulation at CDWs leads to a modification of the energy bands in the BTO, creating an asymmetric saw-teeth potential known to produce the so-called ratchet effect [16, 18]. Namely, it was hypothesized that the illumination might cause nonequilibrium at the CDWs, thereby leading to the motion of domain walls. In this work, a formal description of the light-driven motion of charged domain walls is presented, shedding new insight into the interaction between visible light and ferroelectric order in isolated ferroelectrics.

II. PHOTO-INDUCED ELECTRONIC RECONSTRUCTION MECHANISM

CDWs appear in some ferroelectric materials due to the convergence of the polarization of two adjacent ferroelectric domains [20, 21]. The bound charge is screened with free carriers even when the adjacent domains are insulating. When extrinsic mechanisms (e.g., compensation by oxygen vacancies [22] or additional order parameters like octahedral tilt [23]) are not the most relevant stabilizing agents of charged domain walls, the electronic band-bending mechanism is the only one capable of generating free charges in order to compensate the polarization discontinuity in the walls [20, 24]. As was described, the driving force for this mechanism is the existence of a huge internal electric field (around 2.7 GV/m in BTO at room temperature [25]), which arises from the bound charge accumulated in the walls [26, 27].

Like the electronic reconstruction in oxide interfaces [28], the electronic band-bending mechanism is produced when the distance between domain walls (or domain size) reaches a value above a critical one. In this case, the local valence band in the wall with a positive bound charge is aligned with the local conduction band in the other wall, leading to electron transfer from one type of wall to another. This is similar to a Zener-like breakdown [29] (but without Zener tunnelling), which creates local regions with an accumulation of electrons or holes.

Sluka et al. [24] show that a domain pattern containing CDWs can achieve an equilibrium state through incomplete screening of polarization discontinuity, which

provides an effective electric field inside domains. Because of the alternating sign of consecutive CDWs, the spatial distribution of the depolarization field between walls (or its electric potential) shall be an oscillating function having the maximal or minimal values in the position of the walls. In this way, the group constituted by a domain and two consecutive CDWs (labeled as CDW array) is formed by three main regions: an insulator region associated with the domain, and two n-type and p-type conductivity local regions arising from head-head (positive convergence of polarization) and tail-tail (negative convergence of polarization) CDWs, respectively. From this point of view, a CDW array has a remarkable similarity with artificial semiconductor structures, such as metallic oxide interface with the presence of two-dimensional electron (or hole) gas [30–32] and *nipi*-semimetallic crystals constituted by periodic layers with alternating doping of donors and acceptor impurities embedded in a non-doped host material [33, 34]. In these types of structures, three main features can be observed: (i) spatial modulation of the band edges because of the space charge potential, which is originated from a partial compensation of a particular type of charge concentration; (ii) an efficient separation of photoelectron-photohole pairs under the incidence of light due to the existence of the built-in electric field, which leads to long lifetimes for the photoexcited carriers; (iii) optical transitions with associated energies below the band gap owing to the existence of an indirect gap in the real space as a result of spatial separation between electron a hole states [33–36].

Assuming these characteristics can also be found in a CDW array, two questions emerge: How are electron-hole pairs generated when sub-band gap illumination irradiates on the CDW array? Can the generated carriers be related to changes in polarization and related macroscopic properties? Regarding the first question, in *nipi*-nonsemimetallic crystals, an effective gap lower than the band gap exists [34], but it becomes zero for the semimetallic state resulting in the confinement of free carriers at the interface [35]. Thus, optical transitions are only possible by direct transition or tunneling, the latter being almost unlikely because of the small overlap between the electron and hole states within the forbidden gap region [37]. Because of the band configuration similarity in CDW arrays and *nipi*-semimetallics, the tunneling mechanism can be disregarded for CDW arrays.

Di Gennaro et al. [36] proposed a transition mechanism termed photo-induced electronic reconstruction (PER), which explains the light absorption for radiation energies below the gap, more specifically, the optical absorption in the visible spectrum in a $LaAlO_3/SrTiO_3$ (LAO/STO) heterostructure, whose gap energy is ~ 3.6 eV. According to Di Gennaro et al. [38] the PER mechanism can be understood as a slow photo-promotion process that involves the electron promotion from the LAO initial states with O-character to STO final states with Ti-character, and whose transitions can involve a non negligible overlap between the states. Additionally, since the upturn of the bands is steep (specifically, the band bending upwards in the LAO), the farther initial valence band states are located, the larger is energy lift. In consequence, the reduction of the optical gap is a result of the band being in the polar LAO layer. It is important to highlight that the slow process refers to the fact the photo-excitation is due to low energy photons promoting electrons to the quantum well (within STO) from LAO valence band, in contrast to the high energy photon promoting electron directly from the valence band to the conduction band in the LAO (or STO) layer, which is labeled as a fast promotion process.

The non negligible overlap between the states involved in the optical transitions is at the core of the PER mechanism, which can be understood as follows: The analysis of the STO/LAO band character [39] shows that the states below the Fermi level (E_F) are mainly associates from widely O($2p$) states of the AlO_2 layer, forming the upper valence states within the energy interval $-2\,\mathrm{eV} < E < E_F$, and with the O($2p$) states from the TiO_2 layer, forming the intermediate valence band states localized mainly in the energy range $-3\,\mathrm{eV} < E < -2\,\mathrm{eV}$. Furthermore, the states above E_F are mainly formed by Ti($3d$) orbitals, where bands crossing the Fermi level are associated with the triple degenerate t_{2g} states of Ti($3d$) orbitals of the TiO_2 layer within the interface overlapping with the surface O($2p$) bands of the AlO_2 layer, thereby originating the interface metallicity. As calculated by Rasgoti et al. [40], only few bands cross the Fermi level, while there are a significant number of bands around 2 eV below E_F. Therefore, it can expect that optical absorption results from interband transitions occurring between valence band states and the states at E_F. The character of these transitions allow the absorption over a large spectral domain with low energy photons, thereby giving a strong foundation to the PER mechanism.

The LAO/STO heterostructure is electrically very similar to CDW arrays. Both systems have charged interfaces, free carriers in quantum wells around those interfaces, and internal electric fields arising from the charged (uncompensated) interfaces. Although a demonstration of this type of optical transitions in CDWs requires the full calculation of the band structure, a parallelism between the band structure of STO/LAO interfaces and CDWs stabilized by electron/hole screening can be doubtless established [24, 41]. Thus, the valence band in tetragonal $BaTiO_3$ are mainly dominated by p-orbitals of the oxygen atoms, which is expected due to the large electronegativity of the oxygen as compared with the Ti and Ba atoms[42]. On the other hand, the formation of the conduction band mostly consists of unoccupied d-states of the Ti ion. For the case of head-to-head (HH) CDWs, the bands associated to d-states cross the Fermi level in a similar way to STO/LAO interface, so that this states becomes occupied for electrons giving place to a quantum well [43]. Specifically, the motion of electrons per-

pendicular to the domain wall is quantized such that the electron energy spectrum exhibits a finite number of subbands related to free electron propagation along the wall [44]. A similar situation occur in the case of tail-to-tail (TT) CDWs, where an overlapping between the conduction and valence bands is expected, except in the case of the equivalent O($2p$)-states. This is demonstrated numerically in [23].

Note that, if the (electronic) band gap is calculated between conduction band minimum (CBM) and the valence band maximum (VBM), it turns out to be zero such that the VBM and CBM states do not have to be located at the same spatial region [45]. On the other hand, the local band gap from the valence band to the conduction band associated to the same spatial region is similar to that of the monodomain ferroelectric. These facts along with the existence of a partial depolarization electric field (originated from the partial screened of the bound charge in the walls) should allow optical transitions by low energy photons similar to that happen at the STO/LAO interface.

Thus, assuming the PER mechanism as the responsible phenomenon for the optical absorption in CDWs, a photoexcited electron generated by the optical absorption is then transferred from valence band states in the domains (and sufficiently near the wall) to conduction band states in the quantum well localized within the HH-CDW. Furthermore, since photon absorption creates the same amount of holes and electrons, the holes are drifted towards the TT-CDW by effect of the partial depolarization field, which spread from the HH to the TT walls. Fig. 1 illustrates the photo-generation of electron-hole pairs by the PER mechanism in a CDW array. (Note that this process of charge separation is similar to that in pn-junctions [46, 47].) As a result, it is expected that both the joint action of the localized states in the quantum well (acting like traps) and the hole-drift (due to the internal electric field) hindering the recombination process, leading to very long lifetimes of the photoexcited states while the internal field remains sufficiently uncompensated.

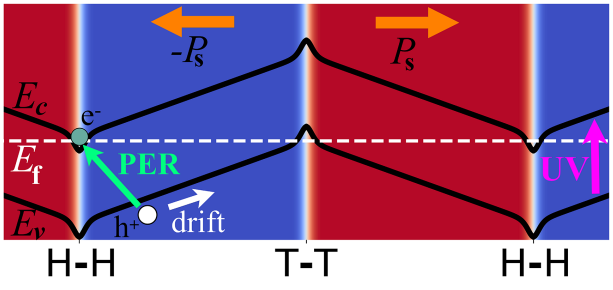

FIG. 1: Schematic representation of the electron-hole pair generation (green arrows) from the valence band to the conduction band in a CDW array by the PER mechanism. White arrow symbolizes the hole drift, orange ones represent the polarization direction, and the terms E_c, E_v, and E_F are the conduction band energy, the valence band energy, and the Fermi level, respectively.

The long lifetime of photo-carriers and the photogenerated charge alter the charge balance at CDWs, leading to a new stable state under illumination. The photo-carriers concentration should be small to modify the local Fermi level of electron and hole gases in the walls. Nevertheless, the effect on the depolarization field can be enough to induce a substantial modification in the band edge profile (note that the value of a partially screened depolarization field is about $10^4\,\mathrm{Vcm}^{-1}$ for a domain size of 3 μm [24]). After the photo-excitation process, the dark state (before illumination) with n_0 and p_0 free carriers in the CDWs is altered so that photo-excited state receives an excess of electron and hole concentrations Δn and Δp, respectively. Therefore, the Fermi level common at both electron and hole concentrations at the dark state (see white dashed line in Fig.1) splits into two quasi-Fermi levels E_F^n and E_F^p for electrons in the HH- and holes in the TT-CDW, respectively.

Positions of E_F^n and E_F^p in the HH- and TT-CDWs are given with respect to the bulk value of E_F in the dark state, leading to the emergence of an effective energy gap E_g^{eff} related to the difference between the quasi-Fermi levels:

$$E_g^{eff} = E_F^n(n_0 + \Delta n) - E_F^p(p_0 + \Delta p). \qquad (1)$$

Since photo-absorption creates the same amount of holes and electrons and considering the light intensity sufficiently weak so that $n_0 \gg \Delta n$, the effective energy gap can be written as:

$$E_g^{eff}(n_0 + \Delta n) \approx \left(\frac{\partial E_g^{eff}}{\partial n}\right)_{n_0} \Delta n. \qquad (2)$$

Consequently, E_g^{eff} turns out to be proportional to the excess charge concentration Δn. Hence, increasing Δn increases the E_g^{eff}, thereby flattening the band edges. To summarize, the photo-excitation process increases the electron and hole concentrations, boosting the screening of CDWs. As a result, the internal electric field decreases. Furthermore, polarization inside the domains and the free energy of the whole system are modified. Undoubtedly, the quantity Δn results to be essential in order to give an estimation about the effect of the light-additional screening, and its impact on the macroscopic properties.

III. PHENOMENOLOGICAL MODEL

If the CDWs are not fully screened, it must there exist available states in the lower conduction band crossing the Fermi level to promote photogenerated electrons by the PER mechanism. Thus, a model describing the dynamics of electrons trapping by the quantum well in the HH-CDW is proposed below, allowing estimating the photogenerated electron concentration Δn, and its relation with the photoinduced electric field. In this

way, the following balance equation is introduced [48]:

$$\begin{cases} \dfrac{d\Delta n}{dt} - G_{ph} + \dfrac{\Delta n(t)}{\tau_h^0} \exp\left(- \dfrac{\Phi(t)}{k_B T} \right) = 0, \\ \Delta n(t=0) = 0 \end{cases} \tag{3}$$

where the recombination term is weighted by a exponential factor. The generation rate G_{ph} can be expressed by:

$$G_{ph} = \frac{I}{\hbar\omega D}, \tag{4}$$

being I the light intensity, $\hbar\omega$ the energy per photon and D the crystal thickness. The function $\Phi(t)$ represents the ease of trapping electrons (that is, the more electron trapped the smaller $\Phi(t)$ will be). Assuming there exists a relationship between $\Phi(t)$ and the electron concentration, $\Phi(t)$ is given from [49] by:

$$\Phi(t) \equiv \Phi_m \frac{\Delta n_m - \Delta n(t)}{\Delta n_m}, \tag{5}$$

being Δn_m the maximum electron excess concentration allowed in the quantum well during photogeneration, and Φ_m the maximum depth of the well that is achieved for full compensation of the bound charge in the wall. The approach given by Sturman et al. [22] is used to determine the value $\Phi_m \approx 0.6\,\text{eV}$ (Appendix A).

A constrain in Δn_m must be introduced to avoid the overcompensation of the charge in the wall, such that $\Delta n_m + n_0 \leq \sigma_b/q\delta_w$ with σ_b the total bound charge in the wall and δ_w the wall thickness. For a partial screened CDW, the difference between the bound charge σ_b and the screening free charge σ_f yields a total bound charge $\sigma_{tot} = \sigma_b - \sigma_f$ different to zero. The existence of σ_{tot} results in a contribution to the free energy $\mathcal{G}$ trough a depolarization field energy expressed as follows [50]:

$$\mathcal{G}_{dep} = -\frac{1}{2}\frac{(\lambda-1)P^2}{\epsilon}, \tag{6}$$

being $\lambda = \sigma_f/\sigma_b$ the screening factor of the bound charge in the wall [51]. Note that $\lambda = 1$ for a full screened wall such that $\mathcal{G}_{dep}$ and, therefore, the depolarization field E_{dep} turn to be zero.

Then, the total free energy can be write out as:

$$\mathcal{G} = \frac{1}{2}\alpha P^2 + \frac{1}{4}\beta P^4 - \frac{1}{2}\frac{(\lambda-1)P^2}{\epsilon}. \tag{7}$$

After transforming $\mathcal{G}$ into a dimensionless form $\mathcal{G}^\star$ by using the dimensionless quantities defined in [52], one gets:

$$\mathcal{G}^\star = \frac{1}{2}\alpha^\star p^2 + \frac{1}{4}\beta^\star p^4 - \frac{1}{2}\frac{(\lambda-1)p^2}{\epsilon^\star}, \tag{8}$$

with $\alpha^\star = -4$, $\beta^\star = 4$ and $\epsilon^\star = (\epsilon_0\epsilon_b E_b/P_0^2) \approx 4.6\times10^{-3}$, where $E_b = |\alpha|/4\beta \approx 5\times10^6\,\text{J/m}^3$ is the energy barrier between two polarization states, $P_0 = 0.26\,\text{Cm}^{-2}$ is the spontaneous polarization, and $\epsilon_b \approx 7$ is the background permittivity for $BaTiO_3$ [24].

To obtain the strength of the depolarization field, $\mathcal{G}^\star$ can be plotted for different λ values. Fig. 2a shows large reduction of the order parameter for $\lambda > \lambda_3$; that is, the depolarization field becomes high enough to destabilize the polarization. Moreover, for $\lambda = \lambda_4$, $\mathcal{G}^\star$ achieves a minimum (Fig. 2a) with an optimal polarization value (Fig.2b).

Calculating the corresponding depolarization field, we obtain:

$$E_{dep} = -\frac{(1-\lambda_4)\sigma_b}{\epsilon^\star P_0} E_0 \approx 1.1\times10^6\,\text{Vm}^{-1} \tag{9}$$

for $BaTiO_3$ with domain size $d = 3\ \mu$m and energy gap $\mathcal{E}_g = 3\,\text{eV}$ [31]. Here, $E_0 = (E_b/P_0) = 1.9\times10^7\,\text{Vm}^{-1}$ is the normalization value of electric field.

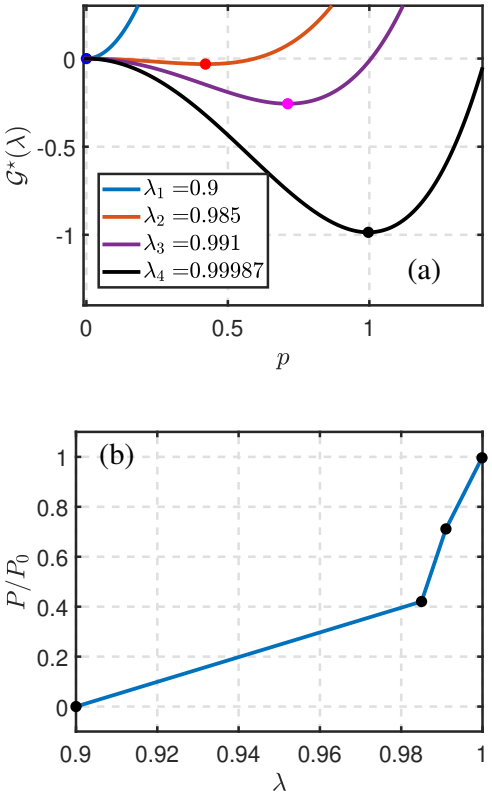

FIG. 2: (a) Dimensionless free energy $\mathcal{G}^\star$ and (b) maximum polarization corresponding to $\mathcal{G}^\star$ minimum for different λ values.

Taking λ_4 to be the screening factor for the dark conditions; then, an additional screening occurs under illumination, such that λ can be written as two contributions:

$$\lambda = \lambda_{dark} + \lambda_{light} \leq 1; \tag{10}$$

so that, a full screening of the wall is reached to $\lambda_{light} = 1 - \lambda_{dark} = 1 - \lambda_4$. Note that, although the value of λ

is small, it becomes enough to produce a modification in the depolarization field.

Once λ_{light} is known, it is possible to estimate the screening surface charge density σ_{ph} needed to obtain a full compensation of CDW; that is,

$$max(\sigma_{ph}) = (1 - \lambda_{dark})\sigma_b \approx 6.7 \times 10^{-9}\,\mathrm{Ccm}^{-2}. \quad (11)$$

Finally, an estimation of the concentration Δn_m can be done as follow [20]:

$$\Delta n_m = \frac{max(\sigma_{ph})}{q\delta_w} \approx 2 \times 10^{16}\,\mathrm{cm}^{-3} \quad (12)$$

which is fourth order smaller than the electron concentration in the CDW before illumination; i.e., $n_0 \approx 10^{20}\mathrm{cm}^{-3}$ [20, 24]. The value of the wall thickness, δ_w, is obtained from Fig. 7b (Appendix A).

Based on the previous calculations, Fig. (3) displays the solution of Eq. (3) for a crystal thickness of 1 mm and a continuous 500 nm of wavelength light impinging on an area of 1 mm^2 with light intensity between $1 - 5\,\mathrm{Wcm}^{-2}$, according to the experimental conditions reported in [17, 18]. As may be observed, Fig. (3) describes the increase of the number Δn of electrons promoted into the HH-CDW after the light is turned on. Note that the full compensation of σ_b is not achieved for the used light intensity interval, which can be understood in terms of the decreasing in E_{dep}. During illumination, electrons are promoting into the quantum well whereby E_{dep} receives an additional screening and, in consequence, the recombination process playing a major role (the efficient electron-hole separation due to E_{dep} is lost). Additionally, the time to achieve the saturation concentration is significatively larger than the required time with upper-band gap illumination ($\sim$ 1 ns) [53], wherewith the model describes a slow promotion process. Furthermore, it is observed an increment of the electron concentration with the light intensity increases, which is related to the increase of photons impinging the sample.

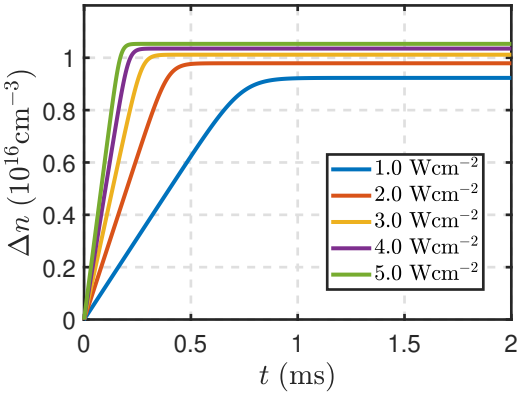

FIG. 3: Time dependence of photogenerated electron excess concentration at different light intensities.

The increasing charge carrier concentration at CDWs by sub-band gap photo-excitation causes an increase ζ_{ph} of the electrical conductivity in the walls (here, sheet conductivity is being considered). Since a proportionality of the photo-conductivity ζ_{ph} with the excess of charge carrier concentration caused by illumination should exist, one has:

$$\zeta_{ph} = \mu \Delta n_{2d}, \quad (13)$$

where μ is the charge carrier mobility at CDWs, which can be considered as a constant and Δn_{2d} the laminar concentration. On the other hand, if the number of photo-excited carriers is proportional to the light intensity (that is, the linear regimen of illumination), a total conductivity dependent on light intensity $\zeta_{tot}(I)$ can be introduced, which is the sum of the dark conductivity $\zeta_{dark} = \zeta_{tot}(I = 0)$ and the photo-conductivity ζ_{ph}.

By expanding into Taylor series, one gets:

$$\zeta_{tot} \approx \zeta_{dark} + \left(\frac{\partial \zeta_{tot}}{\partial I}\right) I. \quad (14)$$

Considering $\zeta_{dark} = \mu n^0_{2d}$, Eq. (14) give rise to:

$$\zeta_{tot} = \mu n_{tot} = \mu n^0_{2d} + \left(\frac{\partial \zeta_{tot}}{\partial I}\right) I, \quad (15)$$

such that the lighting contribution to the screening charge can be obtained as:

$$n_{tot}(I) = n^0_{2d} + \Omega I, \quad (16)$$

being:

$$\Omega = \frac{1}{\mu}\left(\frac{\partial \zeta_{tot}}{\partial I}\right). \quad (17)$$

Note that Ω can be experimentally estimated by measuring the electrical conductivity in the wall under light conditions. However, Ω can be also estimated by using Eq. (16), taking into account the saturation values for $\Delta n(t)$ at different light intensities and calculating Δn_{2d} by Eq. (12). Fig.4 shows a quasi linear relation between Δn_{2d} and I for a light intensity range from $1\,\mathrm{Wcm}^{-2}$ to $5\,\mathrm{Wcm}^{-2}$. At this range, linear relationships for the light intensity dependence of the dielectric and mechanical responses of $BaTiO_3$ have been experimentally observed [17, 18]. Below $1\,\mathrm{Wcm}^{-2}$, the nonlinear behaviour emerges more evident as a result of the dominance of the exponential factor in the recombination term of Eq. (3). A value of $\Omega \approx 10^8\,\mathrm{W}^{-1}$ is obtained from the linear fitting.

As a result of the above relations, the light effect on the Gibbs free energy can be represented by the insertion of a photo-induced energy term working like a driving force [51, 54, 55]:

$$\mathcal{G}_{ph} = \lambda_{light} E_{ph} P, \quad (18)$$

where the photo-induced electric field E_{ph} is given by:

$$E_{ph} = -\frac{q\Omega}{\epsilon_b \epsilon_0} I, \quad (19)$$

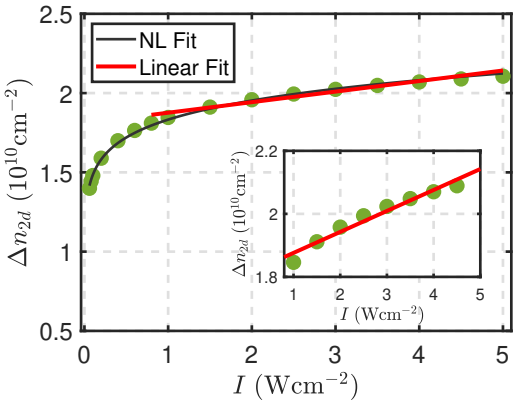

FIG. 4: Relation between the photogenerated laminar electron concentration and the light intensity for a range of $0.06 - 5\,\mathrm{Wcm}^{-2}$. Inset shows the linear fitting for the range of $1 - 5\,\mathrm{Wcm}^{-2}$

which is triggered by the photo-generated charge density $\sigma_{ph} = q\Delta n_{2d}$. The value of the photoinduced electric field for different light intensities in the linear regime is given by

$$E_{ph}(\mathrm{Vm}^{-1}) = -\frac{2q\Omega E_0}{\epsilon^\star \sigma_b} I \approx -2.6 \times 10^4 I. \tag{20}$$

Note that E_{ph} is in the opposite direction of the depolarization field and it is significantly lower than the coercive field.

IV. PHOTO-INDUCED DOMAIN WALL MOTION

Free charges can be created from the electronic band-bending mechanism only whether the distance w between CDWs is greater than a critical distance w_c. Therefore, a correlation between the depolarization field and w should exist. In order to find this relationship, the competition between two energies is considered: the energy cost of the charge transfer across the band gap E_g, and the electrostatic energy making feasible the free charge accumulation in the walls [56]; that is,

$$\Phi(\sigma) = \sigma\Delta - \frac{w}{2\epsilon_0\chi_0}[\sigma_b^2 - (\sigma - \sigma_b)^2], \tag{21}$$

where $\Delta = E_g/q$, χ_0 is the electric susceptibility and σ and σ_b the transferred and bound charge in the walls, respectively.

If E^0_{dep} represents the depolarization field before screening, the internal electric field can be written as:

$$E_{dep}(w) = E^0_{dep} - \frac{\sigma(w)}{\epsilon_0\chi_0}, \tag{22}$$

where $\sigma(w)$ in equilibrium can be obtained from minimizing Eq. (21). That is,

$$\Delta + \frac{w}{\epsilon_0\chi_0}(\sigma - \sigma_b) = 0. \tag{23}$$

Note that in the absence of screening charge (i.e., $\sigma = 0$), the critical distance between walls is:

$$w_c = \frac{\epsilon_0\chi_0\Delta}{\sigma_b}; \tag{24}$$

thus, the expression for the equilibrium carrier density σ_f results:

$$\sigma_f = \sigma_b - \frac{\epsilon_0\chi_0\Delta}{d}. \tag{25}$$

From Eqs. (22) and (24), the correlation between the residual depolarization field and the CDW distance reads:

$$E_{dep}(w) \approx \frac{\Delta}{w}. \tag{26}$$

Therefore, considering different domain sizes (as illustrated in Fig. 5a), adjacent domains are expected to have different values of E_{dep}.

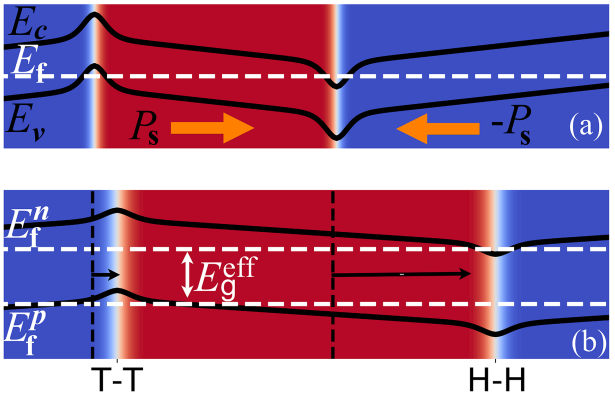

FIG. 5: Schematic representation of an asymmetrical CDW array because of differences in the domain size before (a) and after (b) illumination. Vertical dashed lines are eye guides to highlight the CDW motion.

The driving force to move a domain wall is well-known to be associated with the energetic difference between domains [57]. For instance, by applying an external electric field, one domain becomes energetically more favorable than the other one, thereby promoting the growth of one domain at the expense of the other. This is the usual way to induce a domain wall motion in isolated ferroelectrics. However, an energetic difference between domains can also be established by illuminating an asymmetrical CDW array. Since reducing the depolarization field is not the same in large and small domains (Eq. 5), the Gibbs free energy in the small domains decreases more quickly than in the large ones. Thus, the growth of the small domains becomes favorable together with the corresponding reduction of the other ones. Then, a light-induced motion of the domain wall occurs as illustrated in Fig. 5b. Here, it is important to highlight that the domain reconfiguration would be reversible, since it is a small perturbation of the ground state (dark state).

In order to estimate the wall motion, the velocity of wall v_w can be computed in terms of the light intensity through the following relation (see Appendix B for details):

$$v_w = -\frac{\Lambda\sigma_{tot}}{\Sigma}E_{ph} = \frac{2\Lambda}{\Sigma}\frac{q\Omega E_0}{\epsilon^\star}\lambda_{light}I, \qquad (27)$$

being the mobility coefficient $\Lambda \approx 4\times10^4\,\mathrm{C^2J^{-1}m^{-1}s^{-1}}$ for $BaTiO_3$, and Σ a term that takes into account the spatial variation of the polarization.

Assuming an unchanged polarization profile at the wall over time, the stationary solution describing the uniform domain wall motion can be expressed by a kink-like function in the polarization; that is,

$$p(z,t) = p(z-\nu_w t) \approx -\tanh\left(\frac{z-\nu_w t}{\delta_w/2}\right), \qquad (28)$$

where the tanh-function is obtained by fitting the profile in Fig. (7b).

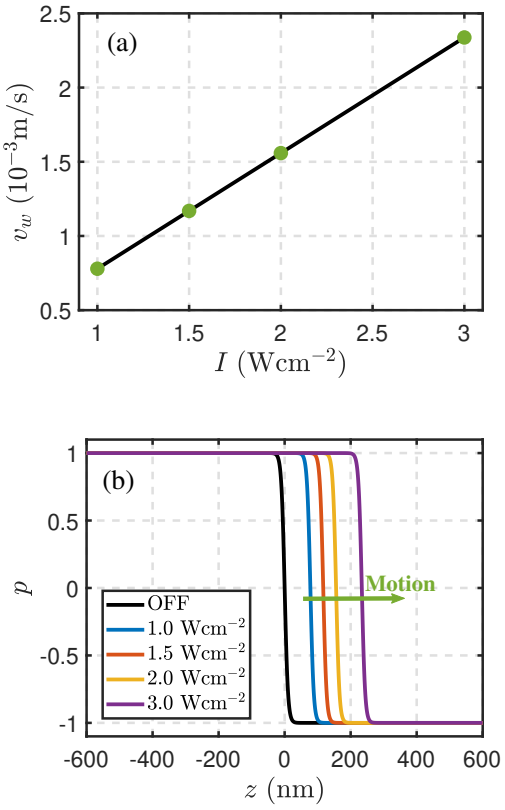

FIG. 6: (a) Light intensity dependence of the domain wall velocity and (b) polarization profile for different light intensities at $t_0 = 1$ ms.

Fig. 6 is obtained by plotting Eqs. (27) and (28) for different light intensities within the linear regime (between $1-3\,\mathrm{Wcm^{-2}}$) according to the experiments [12, 17]. Fig. 6a shows domain wall velocity increase with the light intensity as a result of the increasing of the photoinduced electric field. However, the wall motion is slowly as compared to the values reported for ultra-fast laser-pulse on neutral domain walls [58]. As shown by Gureev et. al. [51] more screening ($\lambda_{light} \to 0$) in CDW turns the wall less sensitive to drive force E_{ph} and, in consequence, the wall dynamics generated by the PER mechanism needs long time to trigger macroscopic changes in the domain configuration. For instance, for a time in which the photoinduced electric field achieve the maximum values (i.e., $t_0 \approx 1$ ms), the distance covered by the wall is around $\sim 10^2$ nm as shown in the Fig. 6b, being this value in agreement with those reported in [12].

V. CONCLUSIONS

Summarizing, the developed phenomenology successfully describes experimental observations on domain wall motion, domains rearrangement, and consequently, linear change of polarization when light with photon energy below the material band gap impinging on an isolated ferroelectric. Experimental observations and physical phenomenology are now bridged. It is put in evidence that visible light modifies CDW compensation such that the depolarization field changes, triggering the domain wall motion. As a result, a rearrangement of the domain structure occurs, leading to a macroscopic polarization variation. Because the CDWs compensation depends linearly on the light intensity, the polarization can be easily tuned, as has been experimentally observed. Our findings provide fundamental insights into the physical attributes that allow light-driven motion of charged domain walls in ferroelectrics, thereby projecting an exciting direction towards the accelerated discovery of new ferroelectric materials for developing the next generation of high-efficiency photo-controlled ferroelectric-based devices.

ACKNOWLEDGMENTS

This work is supported by the AEI (Spanish Government) projects PGC2018-099158-B-I00 and PID2020-114192RB-C41. M.V. acknowledges support from São Paulo Research Foundation FAPESP (grant number 2017/17872-1 and 2022/08030-5) and brazilian CNPq (process 304144/2021-5). J.E.G. whishes to thank the Becas Iberoamérica Santander Investigación 2020-2021 program for their financial support. F.R-M. is indebted to Comunidad de Madrid for the financial support through the "Doctorados Industriales" project (IND2020/IND-17375), which is co-financed by the European Social Fund.

APPENDIX A: DETERMINATION OF THE CONFINEMENT POTENTIAL

Because the high electron concentration in the wall, the Thomas-Fermi (TF) model results a good approximation to obtain the electric confinement potential ϕ. Thus, for a full compensation regime, ϕ can be obtained from both the state equation of polarization (from the Landau theory)

$$-\frac{d\phi}{dz} = \alpha P + \beta P^3, \tag{29}$$

and the general electrostatic relation

$$\frac{dP}{dz} \approx \rho, \tag{30}$$

where P stands for the polarization, α and β are the Landau coefficients and ρ the compensating charge density. In the TF-model, ρ is a function of ϕ expressed by

$$\rho = -\frac{q(2m_e q\phi)^{3/2}}{3\pi^2\hbar^3}, \tag{31}$$

with m_e being the electron effective mass, q the elementary charge and $\hbar$ the reduced Planck's constant.

Mixing Eqs. (29) and (30), and using the boundary conditions $\phi(\infty) = 0$ and $P(\infty) = P_0$, the following conservation law emerges:

$$\frac{|\alpha|P_0^2}{4}\left(1 - \frac{P^2}{P_0^2}\right)^2 + \int_0^{\phi} \rho(\phi')d\phi' = 0, \tag{32}$$

allowing to obtain a relation between P and ϕ. Taking into account Eq. (31), the confinement potential can be obtained by solving

$$\phi = \left[\frac{|\alpha|P_0^2}{4}\frac{6\pi^2\hbar^2}{5q(2m_e q)^{3/2}}\right]^{2/5}\left(1 - \frac{P^2}{P_0^2}\right)^{4/5} \tag{33}$$

and

$$\frac{dP}{dz} = -\frac{q(2m_e q)^{3/2}}{3\pi^2\hbar^2}\times \times\left[\frac{|\alpha|P_0^2}{4}\frac{6\pi^2\hbar^2}{5q(2m_e q)^{3/2}}\right]^{6/10}\left(1 - \frac{P^2}{P_0^2}\right)^{6/5}. \tag{34}$$

Eqs. (33) and (34) can be substantially simplified after a proper normalization by using the dimensionless quantities $d = (2\hbar^2/m_e q|\alpha|P_0)^{1/3}$, $\tilde{z} = z/d$, $p = P/P_0$, and $u = -m_e d^2 q\phi/\hbar^2$ [44], yielding

$$u = -c_1 Q^{2/5}(1 - p^2)^{4/5} \tag{35}$$

and

$$\frac{dp}{d\tilde{z}} = -\frac{c_2}{Q^{2/5}}(1 - p^2)^{6/5}, \tag{36}$$

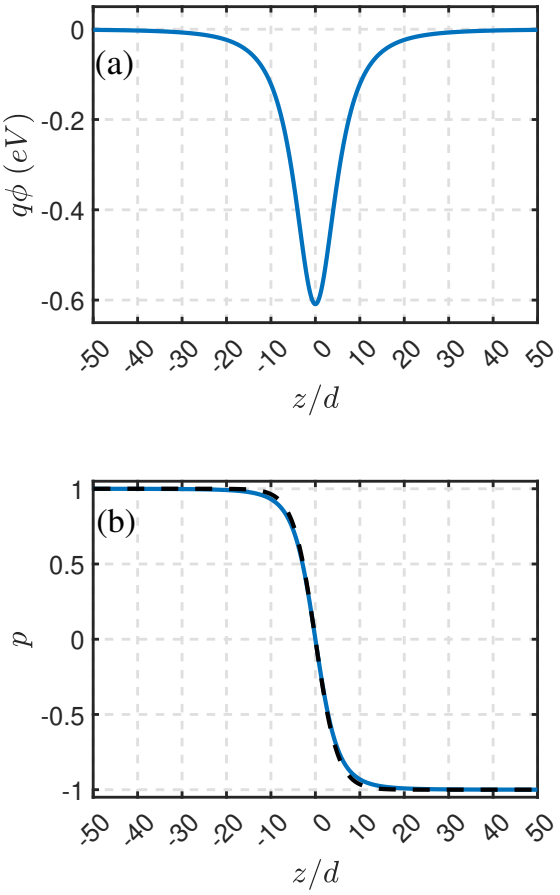

FIG. 7: (a) Confinement potential and, (b) polarization profile in the HH-CDW. The dashed line in (b) is the fitting for $p \approx -\tanh(z/5d)$.

being $c_1 = (15\pi/32\sqrt{2})^{2/5} \approx 1.016$, $c_2 = 8\sqrt{2}c^{3/2}/3\pi \approx 1.23$, and $Q = 4\pi P_0 d^2/q \approx 10^2$.

After solving Eqs. (35) and (36), we can estimate $\Phi_m = |q\phi(0)| \approx 0.6\,\text{eV}$ from Fig. 7a. Additionally, the thickness of wall was estimate to be $\delta_w \approx 20\,\text{nm}$ from Fig. 7b, by taking the tangent to the polarization profile at the center of the wall and measuring the distance between the intersection of the tangent with the $p = \pm 1$. The obtained δ_w agrees with the value estimate by Gureev et al. [20].

APPENDIX B: DETERMINATION OF THE WALL VELOCITY

Under illumination, the internal electric field is disturbed by photogenerated charges into the quantum well within the wall, thereby inducing a reduction in the depolarization field E_{dep}, which can be understood like the effect of a photoinduced field E_{ph} working against E_{dep}. From [59] we can obtain an estimate value for the

wall velocity. Let define an effective free energy density:

$$f_{ef} = \frac{1}{2}\alpha P^2 + \frac{1}{4}\beta P^4 + \frac{1}{2}k_{ef}\left(\frac{dP}{dz}\right)^2 - \frac{(\lambda-1)}{\epsilon_0\epsilon_b}P^2 + \lambda_{light}E_{ph}P, \tag{37}$$

where $k_{ef} = k + k_\rho$ represents the effective gradient coefficient for CDWs as proposed by Gureev et al. [20]. Integrating in a domain of interest Γ, the effective energy $\mathcal{F}_{ef}$ is given as:

$$\mathcal{F}_{ef} = \int_\Gamma f_{ef} d\Gamma = \int_\Gamma (f_{int} + f_{ph}) d\Gamma \equiv \mathcal{F}_{int} + \mathcal{F}_{ph}, \tag{38}$$

showing two contributions: the internal free energy, and a coupling term described by the light-induced modification of the internal field with the polarization, which works like driving force [51].

Due to the domain wall motion, a time rate of energy dissipation is involved, which can be expressed as:

$$\dot{\mathcal{F}}_{diss} = -\int_\Gamma \frac{1}{2}\left[\frac{\delta \mathcal{F}_{ef}}{\delta P}\right] d\Gamma. \tag{39}$$

By using a dissipative dynamics Landau-Khalatnikov type, one gets:

$$\dot{P} = -\Lambda \frac{\delta F_{ef}}{\delta P}, \tag{40}$$

such that Eq. (39) can be rewrite as:

$$\dot{\mathcal{F}}_{diss} = \frac{1}{\Lambda}\int_\Gamma \frac{1}{2}\dot{P}^2 d\Gamma, \tag{41}$$

being Λ a mobility parameter considered a scalar whether the time-evolution of the order parameter is assumed to be isotropic.

Assuming CDW translates with a constant velocity v_w while the wall profile remains unchanged over time (valid for weak photo-induced electric field $E_{ph} < E_{coercive}$), the time derivative of the polarization can be expressed as:

$$\dot{P} = v_w \frac{dP}{dz}, \tag{42}$$

thereby the dissipation rate becomes:

$$\dot{\mathcal{F}}_{diss} = \int_\Gamma \frac{1}{2}\frac{v_w^2}{\Lambda}\left(\frac{dP}{dz}\right)^2 d\Gamma. \tag{43}$$

Taking into account that [59]:

$$\Sigma = \int_\Gamma \left(\frac{dP}{dz}\right)^2 d\Gamma \approx \frac{8P_0^2}{3\delta_w}, \tag{44}$$

it is obtained:

$$\dot{\mathcal{F}}_{diss} = \frac{\nu_w^2 \Sigma}{2\Lambda}. \tag{45}$$

Because only the coupling term depends on the position of domain wall, the change in the free energy comes exclusively from this term, such that:

$$\frac{d}{dt}\mathcal{F}_{ef} = \frac{d}{dt}\int_\Gamma \lambda_{light} P E_{ph} d\Gamma. \tag{46}$$

From Eq. (46) and making use of Eq. (42) we obtain:

$$\frac{d}{dt}\mathcal{F}_{ef} \approx 2P_0 \lambda_{light} E_{ph} v_w = \sigma_{tot} E_{ph} v_w. \tag{47}$$

Finally, the definition of the dynamic energy rate is introduced [59], such as:

$$\dot{\mathcal{F}}_{dyn} = \dot{\mathcal{F}}_{diss} + \frac{d}{dt}\mathcal{F}_{ef} = \frac{v_w^2}{2\Lambda}\Sigma + \sigma_{tot} E_{ph} v_w, \tag{48}$$

leading to the stationary condition:

$$\frac{\partial \dot{\mathcal{F}}_{dyn}}{\partial v_w} = 0. \tag{49}$$

After solving the above equation, an expression for the wall velocity is obtained:

$$v_w = -\frac{\Lambda \sigma_{tot} E_{ph}}{\Sigma} > 0. \tag{50}$$

[1] G. Catalan, J. Seidel, R. Ramesh, and J. F. Scott, Domain wall nanoelectronics, Rev. Mod. Phys. **84**, 119 (2012).

[2] J. Seidel, Nanoelectronics based on topological structures, Nat. Mater. **18**, 188 (2019).

[3] R. Mankowsky, A. von Hoegen, M. Först, and A. Cavalleri, Ultrafast reversal of the ferroelectric polarization, Phys. Rev. Lett. **118**, 197601 (2017).

[4] Y. Ahn, J. Park, A. Pateras, M. B. Rich, Q. Zhang, P. Chen, M. H. Yusuf, H. Wen, M. Dawber, and P. G. Evans, Photoinduced domain pattern transformation in ferroelectric-dielectric superlattices, Phys. Rev. Lett. **119**, 057601 (2017).

[5] M.-M. Yang and M. Alexe, Light-induced reversible

control of ferroelectric polarization in bifeo3, Adv. Mater. **30**, 1704908 (2018).
[6] T. Li, A. Lipatov, H. Lu, H. Lee, J.-W. Lee, E. Torun, L. Wirtz, C.-B. Eom, J. Íñiguez, A. Sinitskii, and A. Gruverman, Optical control of polarization in ferroelectric heterostructures, Nat. Commun. **9**, 3344 (2018).
[7] A. V. Kimel, A. M. Kalashnikova, A. Pogrebna, and A. K. Zvezdin, Fundamentals and perspectives of ultrafast photoferroic recording, Phys. Rep. **852**, 1 (2020).
[8] Y. Bai, Photoresponsive piezoelectrics, Front. Mater. **8**, 636712 (2021).
[9] S. M. Young and A. M. Rappe, First principles calculation of the shift current photovoltaic effect in ferroelectrics, Phys. Rev. Lett. **109**, 116601 (2012).
[10] C. Paillard, X. Bai, I. C. Infante, M. Guennou, G. Geneste, M. Alexe, J. Kreisel, and B. Dkhil, Photovoltaics with ferroelectrics: Current status and beyond, Adv. Mater. **28**, 5153 (2016).
[11] G. Vats, Y. Bai, and J. Seidel, Optomechanical mapping of ferroelectric domains and the piezo-photovoltaic effect in ba- and ni-doped (k0.5na0.5)nbo3, Adv. Photonics Res. **2**, 2100050 (2021).
[12] F. Rubio-Marcos, A. D. Campo, P. Marchet, and J. F. Fernández, Ferroelectric domain wall motion induced by polarized light, Nat. Commun. **6**, 6594 (2015).
[13] Y. Bai, G. Vats, J. Seidel, H. Jantunen, and J. Juuti, Boosting photovoltaic output of ferroelectric ceramics by optoelectric control of domains, Adv. Mater. **30**, 1803821 (2018).
[14] G. Vats, Y. Bai, D. Zhang, J. Juuti, and J. Seidel, Optical control of ferroelectric domains: Nanoscale insight into macroscopic observations, Adv. Opt. Mater. **7**, 1800858 (2019).
[15] Y. Yuan, Z. Xiao, B. Yang, and J. Huang, Arising applications of ferroelectric materials in photovoltaic devices, J. Mater. Chem. A **2**, 6027 (2014).
[16] F. Rubio-Marcos, D. A. Ochoa, A. D. Campo, M. A. García, G. R. Castro, J. F. Fernández, and J. E. García, Reversible optical control of macroscopic polarization in ferroelectrics, Nat. Photonics **12**, 29 (2018).
[17] D. Páez-Margarit, F. Rubio-Marcos, D. A. Ochoa, A. Del Campo, J. F. Fernández, and J. E. García, Light-induced capacitance tunability in ferroelectric crystals, ACS Appl. Mater. Interfaces **10**, 21804 (2018).
[18] F. Rubio-Marcos, D. Páez-Margarit, D. A. Ochoa, A. D. Campo, J. F. Fernández, and J. E. García, Photo-controlled ferroelectric-based nanoactuators, ACS Appl. Mater. Interfaces **11**, 13921 (2019).
[19] F. Rubio-Marcos, A. D. Campo, J. Ordoñez-Pimentel, M. Venet, R. E. Rojas-Hernandez, D. Páez-Margarit, D. A. Ochoa, J. F. Fernández, and J. E. García, Photocontrolled strain in polycrystalline ferroelectrics via domain engineering strategy, ACS Appl. Mater. Interfaces **13**, 20858 (2021).
[20] M. Y. Gureev, A. K. Tagantsev, and N. Setter, Head-to-head and tail-to-tail 180° domain walls in an isolated ferroelectric, Phys. Rev. B **83**, 184104 (2011).
[21] P. S. Bednyakov, B. I. Sturman, T. Sluka, A. K. Tagantsev, and P. V. Yudin, Physics and applications of charged domain walls, npj Comput. Mater. **4**, 65 (2018).
[22] B. Sturman and E. Podivilov, Ion and mixed electron-ion screening of charged domain walls in ferroelectrics, EPL **122**, 67005 (2018).
[23] L. Chen, C. Paillard, H. J. Zhao, J. Íñiguez, Y. Yang, and L. Bellaiche, Tailoring properties of hybrid perovskites by domain-width engineering with charged walls, npj Comput. Mater. **4**, 143201 (2018).
[24] T. Sluka, A. K. Tagantsev, D. Damjanovic, M. Gureev, and N. Setter, Enhanced electromechanical response of ferroelectrics due to charged domain walls, Nat. Commun. **3**, 748 (2012).
[25] P. Ondrejkovic, P. Marton, M. Guennou, N. Setter, and J. Hlinka, Piezoelectric properties of twinned ferroelectric perovskites with head-to-head and tail-to-tail domain walls, Phys. Rev. B **88**, 024114 (2013).
[26] B. M. Vul, G. M. Guro, and I. I. Ivanchik, Encountering domains in ferroelectrics, Ferroelectrics **6**, 29 (1973).
[27] K. Rahmanizadeh, D. Wortmann, G. Bihlmayer, and S. Blügel, Charge and orbital order at head-to-head domain walls in $pbtio_3$, Phys. Rev. B **90**, 115104 (2014).
[28] W.-j. Son, E. Cho, B. Lee, J. Lee, and S. Han, Density and spatial distribution of charge carriers in the intrinsic n-type $laalo_3$-$srtio_3$ interface, Phys. Rev. B **79**, 245411 (2009).
[29] D. R. Småbråten, Q. N. Meier, S. H. Skjærvø, K. Inzani, D. Meier, and S. M. Selbach, Charged domain walls in improper ferroelectric hexagonal manganites and gallates, Phys. Rev. Materials **2**, 114405 (2018).
[30] N. C. Bristowe, E. Artacho, and P. B. Littlewood, Oxide superlattices with alternating p and n interfaces, Phys. Rev. B **80**, 045425 (2009).
[31] T. Sluka, A. K. Tagantsev, P. Bednyakov, and N. Setter, Free-electron gas at charged domain walls in insulating BaTiO3, Nat. Commun. **4**, 1808 (2013).
[32] I. V. Maznichenko, S. Ostanin, A. Ernst, J. Henk, and I. Mertig, Formation and tuning of 2d electron gas in perovskite heterostructures, Phys. Status Solidi B **257**, 1900540 (2019).
[33] G. Döhler and K. Ploog, Periodic doping structure in GaAs, Prog. Cryst. Growth Charact. **2**, 145 (1979).
[34] K. Ploog and H. Künzel, Growth and properties of new artificial doping superlattices in GaAs, Microelectron. J. **13**, 5 (1982).
[35] K. Ploog and G. H. Döhler, Compositional and doping superlattices in III-v semiconductors, Adv. Phys. **32**, 285 (1983).
[36] E. D. Gennaro, U. S. di Uccio, C. Aruta, C. Cantoni, A. Gadaleta, A. R. Lupini, D. Maccariello, D. Marré, I. Pallecchi, D. Paparo, P. Perna, M. Riaz, and F. M. Granozio, Persistent photoconductivity in 2d electron gases at different oxide interfaces, Adv. Opt. Mater. **1**, 834 (2013).
[37] G. H. Döhler, H. Künzel, and K. Ploog, Tunable absorption coefficient in gaas doping superlattices, Phys. Rev. B **25**, 2616 (1982).
[38] E. D. Gennaro, U. Coscia, G. Ambrosone, A. Khare, F. M. Granozio, and U. S. di Uccio, Photoresponse dynamics in amorphous-LaAlO3/SrTiO3 interfaces, Sci. Rep. **5**, 8393 (2015).
[39] R. Pentcheva and W. E. Pickett, Avoiding the polarization catastrophe in $laalo_3$ overlayers on $srtio_3(001)$ through polar distortion, Phys. Rev. Lett. **102**, 107602 (2009).
[40] A. Rastogi, J. J. Pulikkotil, S. Auluck, Z. Hossain, and R. C. Budhani, Photoconducting state and its perturbation by electrostatic fields in oxide-based two-dimensional electron gas, Phys. Rev. B **86**, 075127 (2012).
[41] X. Wu and D. Vanderbilt, Theory of hypothetical fer-

roelectric superlattices incorporating head-to-head and tail-to-tail 180° domain walls, Phys. Rev. B **73**, 020103 (2006).
[42] V. Mishra, A. Sagdeo, V. Kumar, M. K. Warshi, H. M. Rai, S. K. Saxena, D. R. Roy, V. Mishra, R. Kumar, and P. R. Sagdeo, Electronic and optical properties of batio3 across tetragonal to cubic phase transition: An experimental and theoretical investigation, J. Appl. Phys. **122**, 065105 (2017).
[43] P. Bednyakov, B. Sturman, and T. Sluka, Physics and applications of charged domain walls., npj Comput. Mater. **4**, 2057 (2018).
[44] B. Sturman, E. Podivilov, M. Stepanov, A. Tagantsev, and N. Setter, Quantum properties of charged ferroelectric domain walls, Phys. Rev. B **92**, 214112 (2015).
[45] U. Petralanda, M. Kruse, H. Simons, and T. Olsen, Oxygen vacancies nucleate charged domain walls in ferroelectrics, Phys. Rev. Lett. **127**, 117601 (2021).
[46] E. Assmann, P. Blaha, R. Laskowski, K. Held, S. Okamoto, and G. Sangiovanni, Oxide heterostructures for efficient solar cells, Phys. Rev. Lett. **110**, 078701 (2013).
[47] B. Lipovšek, F. Smole, M. Topič, I. Humar, and A. R. Sinigoj, Driving forces and charge-carrier separation in p-n junction solar cells, AIP Adv. **9**, 055026 (2019).
[48] J. Biscaras, S. Hurand, C. Feuillet-Palma, A. Rastogi, R. C. Budhani, N. Reyren, E. Lesne, J. Lesueur, and N. Bergeal, Limit of the electrostatic doping in two-dimensional electron gases of LaXO3(x = al, ti)/SrTiO3, Sci. Rep. **4**, 6788 (2014).
[49] L. Wang, X. Chen, G. Wu, W. Guo, S. Cao, K. Shang, and W. Han, The mechanism of persistent photoconductivity induced by minority carrier trapping effect in ultraviolet photo-detector made of polycrystalline diamond film, Thin Solid Films **520**, 752 (2011).
[50] P. Zhou, B. Zeng, W. Yang, J. Liao, F. Meng, Q. Zhang, L. Gu, S. Zheng, M. Liao, and Y. Zhou, Intrinsic 90° charged domain wall and its effects on ferroelectric properties, Acta Mater. **232**, 117920 (2022).
[51] M. Y. Gureev, P. Mokrý, A. K. Tagantsev, and N. Setter, Ferroelectric charged domain walls in an applied electric field, Phys. Rev. B **86**, 104104 (2012).
[52] Y. Xiao, V. B. Shenoy, and K. Bhattacharya, Depletion layers and domain walls in semiconducting ferroelectric thin films, Phys. Rev. Lett. **95**, 247603 (2005).
[53] B. Sturman and E. Podivilov, Charged domain walls under super-band-gap illumination, Phys. Rev. B **95**, 104102 (2017).
[54] B. Kundys, M. Viret, C. Meny, V. Da Costa, D. Colson, and B. Doudin, Wavelength dependence of photoinduced deformation in bifeo$_3$, Phys. Rev. B **85**, 092301 (2012).
[55] C. Paillard, S. Prosandeev, and L. Bellaiche, Ab initio approach to photostriction in classical ferroelectric materials, Phys. Rev. B **96**, 045205 (2017).
[56] N. C. Bristowe, P. Ghosez, P. B. Littlewood, and E. Artacho, The origin of two-dimensional electron gases at oxide interfaces: insights from theory, J. Phys.: Condens. Matter **26**, 143201 (2014).
[57] D. Schrade, R. Mueller, D. Gross, T. Utschig, V. Shur, and D. Lupascu, Interaction of domain walls with defects in ferroelectric materials, Mech. Mater. **39**, 161 (2007).
[58] T. Yang, B. Wang, J.-M. Hu, and L.-Q. Chen, Domain dynamics under ultrafast electric-field pulses, Phys. Rev. Lett. **124**, 107601 (2020).
[59] M. Flaschel and L. De Lorenzis, Calibration of material parameters based on 180 and 90 ferroelectric domain wall properties in ginzburg–landau–devonshire phase field models., Arch. Appl. Mech. **90**, 2755–2774 (2020).